Energy & Environmental Science

# Solar Photoelectrochemical Synthesis of Electrolyte-free $H_2O_2$ Aqueous Solution without Needing Electrical Bias and $H_2$



| | |
|---|---|
| Journal: | *Energy & Environmental Science* |
| Manuscript ID | EE-ART-11-2020-003567.R2 |
| Article Type: | Paper |
| Date Submitted by the Author: | 02-Mar-2021 |
| Complete List of Authors: | Jeon, Taehwa; Pohang University of Science and Technology, Division of Environmental Science and Engineering; Rice University, Department of Civil and Environmental Engineering<br>Kim, Bupmokim; Pohang University of Science and Technology, Division of Environmental Science and Engineering<br>Kim, Chuhyung; Pohang University of Science and Technology, Division of Environmental Science and Engineering<br>Xia, Chuan; Rice University, Department of Chemical and Biomolecular Engineering<br>Wang, Haotian; Rice University, Department of Chemical and Biomolecular Engineering<br>Alvarez, Pedro; Rice University, Department of Civil and Environmental Engineering<br>Choi, Wonyong; Pohang University of Science and Technology, Division of Environmental Science and Engineering |
| | |

## Broader Context

The current industrial production process of $H_2O_2$ that is energy-intensive and environmentally unsustainable has motivated the search of alternative methods of greener production. Photoelectrochemical (PEC) system is an eco-friendly method that uses sunlight, water and dioxygen only without using $H_2$ gas. Herein we develop a new PEC-based system to produce pure aqueous $H_2O_2$ solution free from electrolytes. The proposed system is based on a three-compartment-stack cell, which consists of $RuO_x$-loaded $TiO_2$ nanorod photoanode, anthraquinone-anchored cathode, and solid polymer electrolyte (SPE). Engineering of both photoanode and cathode achieves a successful system operation at a bias-free condition with high efficiency and durability. The SPE in a middle cell that is located between the photoanode and the cathode facilitates selective transports of $H^+$ and $HO_2^-$ ions that are generated from water oxidation and oxygen reduction on the photoanode and the cathode, respectively, to produce pure (electrolyte-free) $H_2O_2$ solution. The overall photosynthesis process needs water and dioxygen only without external electrical bias and $H_2$ gas.

ARTICLE

# Solar Photoelectrochemical Synthesis of Electrolyte-free $H_2O_2$ Aqueous Solution without Needing Electrical Bias and $H_2$

Tae Hwa Jeon,[a,c] Bupmo Kim,[a] Chuhyung Kim,[a] Chuan Xia,[b] Haotian Wang,[b] Pedro J.J. Alvarez*[c] and Wonyong Choi*[a]

Received 00th January 20xx,
Accepted 00th January 20xx

DOI: 10.1039/x0xx00000x

The conventional synthesis of hydrogen peroxide ($H_2O_2$) such as heterogeneous catalytic and electrochemical processes needs $H_2$ and $O_2$ as reagents, costly noble metals, and organic solvents, which are energy/waste-intensive and hazardous. An alternative method of photoelectrochemical (PEC) synthesis that needs water and sunlight only is environment-friendly but limited for its practical applications due to the need of energy-demanding separation of synthesized $H_2O_2$ from the electrolytes. Herein, we demonstrated the direct synthesis of electrolyte-free aqueous solution of pure $H_2O_2$ by developing a PEC system with solid polymer electrolyte (SPE) and engineered electrodes. Ruthenium catalysts-decorated $TiO_2$ nanorods (RuOx/TNR: photoanode) and anthraquinone-anchored graphite rods (AQ/G: cathode) are placed in an anode and a cathode compartment, respectively, while a middle compartment containing SPE is located between these compartments. Upon solar simulating irradiation (AM 1.5G, 100 mW $cm^{-2}$), the photoanode generated $H^+$ ions via water oxidation reaction (WOR) and the cathode generated $HO_2^-$ ions via two-electron oxygen reduction reaction (ORR), while the SPE selectively transports $H^+$ and $HO_2^-$ into the middle compartment to form pure $H_2O_2$ solution. The combined system enabled continuous $H_2O_2$ synthesis over 100 h even under a bias-free (0.0 V of cell voltage) condition with producing ~80 mM (electrolyte-free) and the Faradaic efficiency of ~90%, which is the highest concentration of pure $H_2O_2$ obtained using PEC systems. This study successfully demonstrates the proof-of-concept that might enable the production of concentrated pure (electrolyte-free) aqueous solution of $H_2O_2$ using sunlight, water, and dioxygen only.

## Introduction

Hydrogen peroxide ($H_2O_2$) is versatile chemical that is widely used in chemical synthesis, cosmetics and medicine, pulp and paper production, and wastewater treatment.[1-5] At present, industrial synthesis of $H_2O_2$ proceeds through hydrogenation of anthraquinone (AQ) with $H_2$ and subsequent oxidation by $O_2$ in organic solvent is a multi-step process that requires high energy input and noble metal catalysts.[6,7] In addition, it generates hazardous solvent wastes. Direct synthesis of $H_2O_2$ from $H_2$ and $O_2$ has emerged as an alternative process for low-cost and decentralized synthesis.[8-10] However, the low production rate of $H_2O_2$, the need for subsequent $H_2O_2$ purification, and safety concerns related to handling potentially explosive $H_2$ and $O_2$ gases pose major challenges for practical use. Therefore, novel environmentally benign and facile methods for $H_2O_2$ synthesis are needed.

Photoelectrochemical (PEC) synthesis of $H_2O_2$ via water oxidation and dioxygen reduction has received growing attention as an alternative green method.[11-14] Reductive and oxidative pathways for PEC synthesis of $H_2O_2$ are based on the oxygen reduction reaction (ORR) by a two-electron transfer (*i.e.*, $O_2/H_2O_2$, $E^o$ = 0.68 V)[15] and the water oxidation reaction (WOR) by a two-electron transfer (*i.e.*, $H_2O_2/H_2O$, $E^o$ = 1.76 V).[16,17] The selective two-electron reduction of $O_2$ to produce $H_2O_2$ is being intensively investigated by using various photocatalysts that include metal oxides and carbon nitrides.[18-21] Based on these fundamental redox reactions, extensive studies have focused on the development of various catalysts to improve selectivity and efficiency, and have demonstrated the capability of PEC system for $H_2O_2$ synthesis via photoanodic, cathodic, or dual photoanodic-cathodic processes.[12,22-26] However, the concentration of $H_2O_2$ synthesized with the PEC system has been limited to a few milli-molar, which impedes practical implementation. Additional challenges that the PEC system faces for practical applications are the separation and purification of synthesized $H_2O_2$. Current PEC systems for $H_2O_2$ synthesis usually need high concentration of electrolytes (summarized in Table S1). However, no PEC study has demonstrated production of electrolyte-free $H_2O_2$ solution due to the difficulty of separating $H_2O_2$ from electrolytes. Therefore, an additional process to purify as-synthesized $H_2O_2$ from electrolytes in PEC cell is needed.

Recently, direct synthesis of pure $H_2O_2$ solution has been achieved using solid polymer electrolyte (SPE) electrolysis cell.[27-31] The utilization of SPE enables the synthesis of pure $H_2O_2$ without any ionic impurities. Wang's group recently reported

[a] Division of Environmental Science and Engineering, Pohang University of Science and Technology (POSTECH), Pohang 37673, Korea. E-mail: wchoi@postech.edu
[b] Department of Chemical and Biomolecular Engineering, Rice University, Houston, TX 77005, USA
[c] Department of Civil and Environmental Engineering, Rice University, Houston, TX 77005, USA
Electronic Supplementary Information (ESI) available. See DOI: 10.1039/x0xx00000x

direct electrochemical synthesis of pure $H_2O_2$ solution via independent electrochemical reaction of $H_2$ and $O_2$ streams, followed by the ionic recombination process leading to the production of $H_2O_2$.[32] The SPE layer placed between an anode and a cathode facilitates recombination of $H^+$ and $HO_2^-$ ions crossing from the anode and cathode compartments, respectively, and deionized (DI) water flowing into the SPE layer dissolves pure $H_2O_2$ formed by recombination of $H^+$ and $HO_2^-$ ions. In contrast with the previous studies that employed SPE,[27-31] they used a catalyst-coated gas diffusion layer electrode to enable direct oxidation of $H_2$ gas on the anode and achieved notably high $H_2O_2$ concentration of ~20 wt% and Faradaic efficiencies (FEs) ~ 90%. This approach offers an attractive route for the synthesis of pure $H_2O_2$ solution.

Here, we applied the SPE design to a PEC system for direct synthesis of pure (electrolyte-free) $H_2O_2$ solution from water and $O_2$ only (without $H_2$) under solar irradiation (Scheme 1 and Figure S1). The $RuO_x$-deposited $TiO_2$ nanorods ($RuO_x$/TNR) photoanode initiates WOR to produce $H^+$ ions upon irradiation, and $HO_2^-$ ions are produced on the AQ-anchored graphite rod (AQ/G) cathode via ORR. The SPE-containing middle compartment facilitates selective transport of $H^+$ and $HO_2^-$, and flowing DI water into the middle compartment dissolves the in-situ generated $H_2O_2$. By modifying both photoanode and cathode, continuous photosynthesis of $H_2O_2$ was achieved under bias-free (0.0 V cell voltage) condition over 100 h. The present study successfully achieved the highest concentration of pure $H_2O_2$ and the longest durability among all the reported PEC works of $H_2O_2$ synthesis (*see* Table S1). Since this PEC system requires only water and $O_2$ (no need for $H_2$ unlike the electrochemical synthesis requiring $H_2$ gas[32]) with sunlight as sole energy source, a sustainable and environmentally benign method is successfully demonstrated for the synthesis of $H_2O_2$.

## Experimental

### Fabrication of photoanodes and cathodes

$TiO_2$ nanorods (denoted as TNR) photoanodes were fabricated on fluorine-doped tin oxide substrates (FTO, Pilkington, 15 Ω square$^{-1}$) via a hydrothermal method.[33,34]

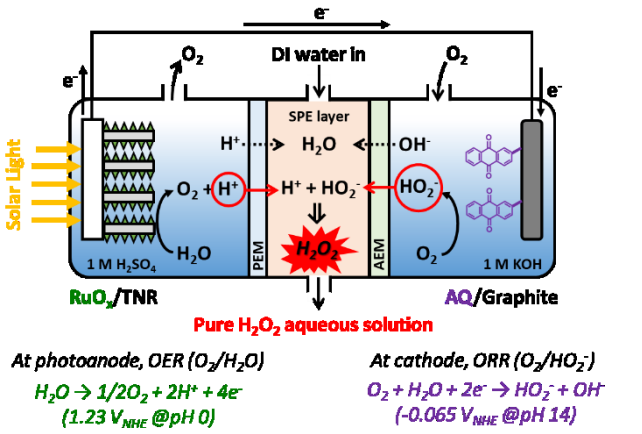


**Scheme 1**. Solar-driven synthesis of pure $H_2O_2$ aqueous solution using a photoelectrochemical cell with solid polymer electrolyte (SPE) in the absence of the applied electrical bias.

Briefly, the two pieces of FTO slides (1 x 1 or 2 x 2 cm$^2$) were vertically placed while the conductive sides faced the wall in a Teflon-lined stainless steel autoclave (total 100 mL volume) containing 25 mL HCl (Aldrich, 37%), 1 mL titanium(IV) butoxide (Aldrich, 97%), and 25 mL deionized (DI) water (18.3 MΩ cm, Barnstead EASYpure RO system). The autoclave was placed in a pre-heated oven at 170 °C for 6 h, and then cooled to room temperature. As-synthesized samples were rinsed with DI water and dried in air, followed by annealing at 550 °C for 1 h with a ramping rate of 10 °C min$^{-1}$. To synthesize $RuO_x$-deposited TNR (denoted as $RuO_x$/TNR) photoanodes, 10 μL cm$^{-2}$ of $RuCl_3$ (10 mM, Aldrich, 99.98%) in ethanol (J.T. Baker, 99.9%) was drop-cast onto as-annealed TNR samples. After drying at room temperature in air for 30 min, samples were immersed in 0.1 M KOH solution for 1 min to form oxides. $FeNiO_x$ and $CoO_x$-deposited TNR (denoted as $FeNiO_x$/TNR and $CoO_x$/TNR) photoanodes were fabricated using the same preparation procedure of $RuO_x$/TNR except for the metal precursors. The solution containing either 4 mM $FeCl_2$ + 6 mM $NiCl_2$ or 10 mM $CoCl_2$ in ethanol was prepared for $FeNiO_x$ and $CoO_x$, respectively, prior to the deposition process. The graphite rod (Aldrich, diameter 6 mm, 99.995%) was directly employed as a cathode substrate without further purification. AQ-anchored graphite rod (denoted as AQ/G) cathodes were synthesized via a simple solution immersion process. Typically, a graphite rod (denoted as G) was immersed in ethanol containing anthraquinone-2-carboxylic acid (AQ-2-COOH, 3 mM, Aldrich, 98%) for 24 h, and dried at room temperature in air.

### (Photo)Electrochemical measurements and analysis

The (photo)electrochemical performances of $RuO_x$/TNR and AQ/G electrodes were conducted in a typical three-electrode system using an electrochemical workstation (VersaSTAT 3-400, Princeton Applied Research) with a two-compartment cell separated by a proton exchange membrane (Nafion Membrane N117) containing 1 M $H_2SO_4$ and 1 M KOH in an anode and a cathode compartment, respectively. A Pt foil and a Ag/AgCl electrode were used as a counter and a reference electrode, respectively, and when needed, a Hg/HgO electrode was also used as an alternative reference electrode. The Ag/AgCl electrode was immersed in the anode compartment. Cyclic voltammograms (CVs) of bare and modified graphite rods were obtained in the range of 0.06 to -1.06 V (vs. Hg/HgO) at a scan rate of 50 mV s$^{-1}$ in the dark. The solutions were purged with Ar (99.9%) or $O_2$ (99.9%) gas for at least 30 min prior to and during the measurements. A constant potential (-0.14, -0.24, -0.34, -0.44, or -0.54 V vs. Ag/AgCl) was applied to bare G or AQ/G electrode, while measuring the amounts of synthesized $H_2O_2$ in the cathode compartment. Linear sweep voltammograms (LSVs) of bare and modified TNR samples were obtained in the range of -0.20 to +1.80 V (vs. Ag/AgCl) at a scan rate of 50 mV s$^{-1}$ in the dark and under simulated sunlight (AM 1.5G, 100 mW cm$^{-2}$). A constant potential (+0.80, +1.30, and +1.80 V vs. Ag/AgCl) was applied to bare TNR or $RuO_x$/TNR electrode, while measuring $O_2$ evolution in the headspace of the anode

compartment. The solution was purged with Ar gas for 30 min prior to the reaction.

For PEC synthesis of $H_2O_2$, a three-compartment-stack system was adopted to combine WOR and ORR. The stacked cell was composed of an anode compartment with photoanode (i.e., TNR or $RuO_x$/TNR) in 1 M $H_2SO_4$ solution; a middle compartment filled with polystyrene crosslinked with divinylbenzene microspheres (Aldrich, 6.0-10.0 μm size) as a solid polymer electrolyte through which DI water flowed; a cathode compartment with a cathode (i.e., bare G or AQ/G) in 1 M KOH solution purged with $O_2$ gas. A proton exchange membrane (PEM, Nafion Membrane N117) and an anion exchange membrane (AEM, AMI-7001S, Membrane International) were placed between the anode and the middle compartments and between the middle and the cathode compartment, respectively (Scheme 1). The Ag/AgCl electrode was immersed in the anode compartment. LSVs of the photoanode-SPE-cathode unit with various configurations (i.e., TNR||SPE||G, TNR||SPE||AQ/G, $RuO_x$/TNR||SPE||G, and $RuO_x$/TNR||SPE||AQ/G) were obtained in the range of -0.20 to +1.80 V (vs. Ag/AgCl) at a scan rate of 50 mV $s^{-1}$ under simulated sunlight (AM 1.5G, 100 mW $cm^{-2}$). A constant potential (+0.80, +1.30, or +1.80 V vs. Ag/AgCl) was applied to TNR or $RuO_x$/TNR electrode, while measuring $H_2O_2$ in the middle compartment. If necessary, a two-electrode system without Ag/AgCl reference electrode was also adopted in the same three-compartment-stack system by applying 0.0 V of cell voltage between the photoanode and cathode electrodes.

For electrochemical rotating ring-disk electrode (RRDE) voltammograms, Pt ring/glassy carbon disk working electrode (ring OD 7 mm/ID 5 mm, disk ID 4 mm, ALS Co., no. 012613), a Pt wire counter electrode, and a Ag/AgCl reference electrode were placed in a single cell containing 0.1 M KOH (pH 13). The bare G and AQ/G samples were ground in a mortar to obtain fine powder, and 30 mg powder and 12 μL Nafion solution (Aldrich, 5 wt% in a mixture of lower aliphatic alcohols and water (40%)) were dissolved and well dispersed in 1 mL ethanol by sonication for 30 min. An aliquot of 5 μL mixture solution was drop-cast onto the glassy carbon disk and dried at room temperature for 10 min. The above drop-casting process was repeated up to 3 times. LSVs of bare G and AQ/G were obtained in the range of 0.0 to -0.6 V (vs. Ag/AgCl) with a scan rate of 10 mV $s^{-1}$ using an electrochemical workstation with bi-potentiostat mode. The solution was pre-purged with $O_2$ gas for at least 30 min prior to and during the measurements. The rotation speed was varied from 100 to 1600 revolutions per minute (rpm) using a rotating ring disk electrode rotator (RRDE-3A, ALS Co., Ltd).

The amounts of synthesized $H_2O_2$ and $HO_2^-$ were quantified using iodometric titration method. For $H_2O_2$, 0.50 mL sample aliquot was mixed with 1.50 mL DI water, 0.75 mL $C_8H_5KO_4$ (0.1 M potassium biphthalate, Alfa Aesar, 98%) solution, and 0.75 mL KI (0.4 M, Aldrich, 99.5%) solution containing NaOH (0.06 M) and $(NH_4)_2MoO_4$ ($10^{-4}$ M, Aldrich, 99%). After vigorous stirring for 2 min, the absorbance was measured at 372 nm using a UV/Visible spectrophotometer (Libra S22, Biochrom). For $HO_2^-$, the same procedure was followed except for the addition of 0.10 mL HCl (1 M) to the above solution, and 1.40 mL of DI water was added instead. The Faradaic efficiency (FE) for $H_2O_2$ or $HO_2^-$ synthesis was calculated by the following: FE = ($2Fn$ / $Q_{ph}$) × 100%, where $F$ is the Faraday constant, n is the measured amount of evolved $H_2O_2$ or $HO_2^-$ (mol), and $Q_{ph}$ is the integrated photocharge.

While applying a constant potential to the working electrode, the amount of evolved $O_2$ was quantified in the headspace of the working electrode compartment using a gas chromatograph (GC, HP6890A) equipped with a thermal conductivity detector (TCD) and a 5 Å molecular sieve column. Prior to irradiation, the solution in the working electrode compartment was purged with Ar gas for 30 min to remove dissolved oxygen. During the measurements, 100 μL of gas sample was intermittently withdrawn from the working electrode headspace with a gastight glass syringe (Hamilton 81030). The FE for $O_2$ evolution was calculated by the following: FE = ($4Fn$ / $Q_{ph}$) × 100%, where $F$ is the Faraday constant, n is the measured amount of evolved $O_2$ (mol), and $Q_{ph}$ is the integrated photocharge.

### Surface characterization

The surface morphologies of TNR and $RuO_x$/TNR were analyzed using high resolution field emission scanning electron microscopy (FE-SEM, JOEL JSM-7800F PRIME) with dual energy dispersive X-ray spectroscopy (EDS) at National Institute for Nanomaterials Technology (Pohang, Korea). X-ray diffraction (XRD) patterns of the samples were measured using Cu Kα radiation (RIGAKU D MAX 2500). X-ray photoelectron spectroscopy (XPS) was analyzed using monochromated Al Kα radiation as an X-ray source (1486.6 eV) at Korea Basic Science Institute (Busan Center, Korea). All XPS peak binding energies were referenced against the adventitious C 1s peak. The surface functional groups of the samples were analyzed by attenuated total reflectance Fourier transform infrared spectroscopy (ATR-FTIR; Thermo Scientific iS50) using a ZeSe crystal with a scan number of 100. The bare G and AQ/G powder samples were obtained by grounding in a mortar.

## Results and discussion

### Highly selective 2-electron reduction of $O_2$ on anthraquinone-anchored graphite rod

The Fourier transform infrared (FT-IR) spectra of bare graphite rod (G) and AQ-anchored graphite rod (AQ/G) samples revealed the presence of anthraquinone in AQ/G sample (Fig. 1a). The IR spectrum of the AQ/G sample exhibited the apparent peaks of AQ at 696, 1267, 1666, and 1701 $cm^{-1}$, indicating the presence of AQ on the graphite rod that was anchored by a simple solution immersion process, while the bare graphite rod exhibited no peaks of AQ. The electrochemical (EC) performance of G and AQ/G samples was investigated using cyclic voltammetry (CVs) in 1 M KOH (pH ~13.6) solution purged with Ar or $O_2$ gas (Fig. 1b). The graphite rod was used as a cathode substrate since it exhibited superior EC activity when anchored with AQ among different carbon-based substrates

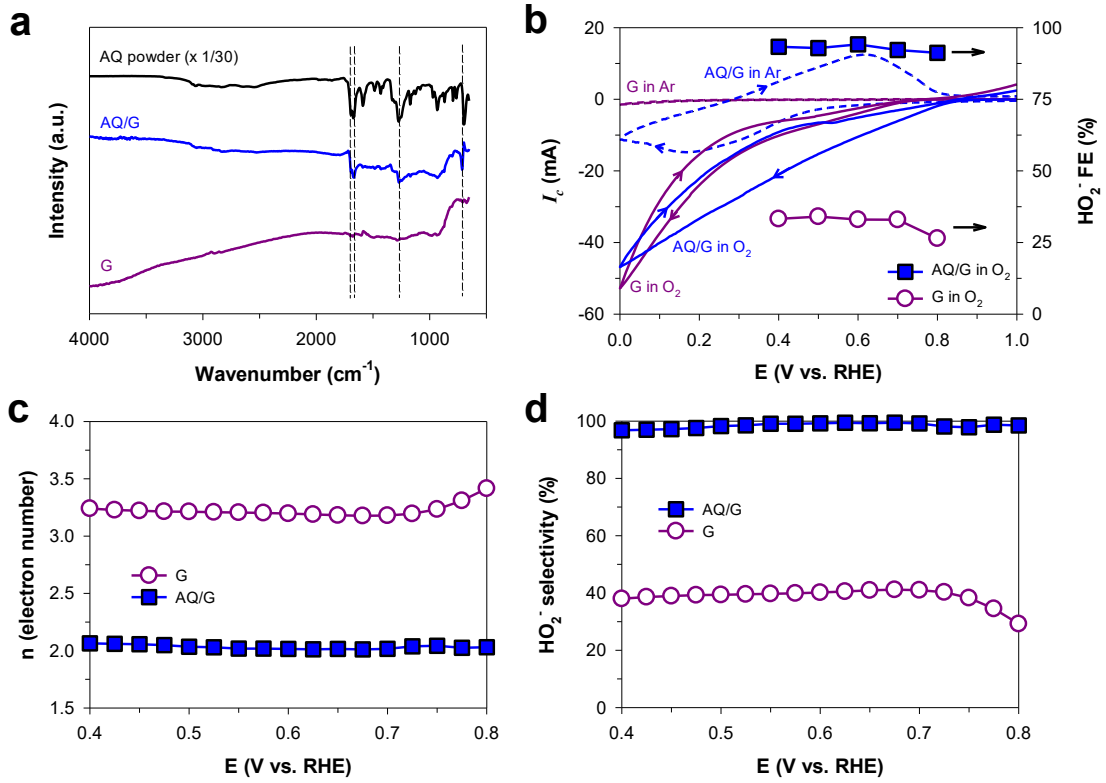


**Figure 1**. (a) FTIR spectra of bare graphite rod (G) and anthraquinone-modified graphite rod (AQ/G). For comparison, the spectrum of anthraquinone (AQ) powder is also shown. (b) Cyclic voltammograms (CVs) of bare G and AQ/G under Ar and $O_2$ in 1 M KOH and Faradaic efficiencies (FEs) for $HO_2^-$ production. (c) The number of electrons transferred on the cathode and (d) the selectivity for $HO_2^-$ with bare G and AQ/G at different potentials, which were obtained from RRDE experiments. See Figure S2 for RRDE disk and ring currents recorded.

(Fig. S2). The CV scan of AQ/G samples under Ar gas exhibited typical peaks of two-electron redox process of anthraquinone/anthrahydroquinone (AQ/AHQ), corroborating the presence of AQ molecules on the graphite rod, while bare G did not exhibit such peaks.[12,35,36]

Upon $O_2$ purging, AQ/G samples exhibited significant reduction currents with an onset potential of +0.8 $V_{RHE}$ for ORR, while bare G exhibited lower ORR currents. The FE for EC $H_2O_2$ synthesis in each potential was calculated based on the amount of synthesized $HO_2^-$ on G and AQ/G, which was measured by sampling the solution in the cathode compartment. The ORR leads to the generation of $H_2O_2$ and $HO_2^-$ as a product in acidic and alkaline condition, respectively.[37,38] Since EC performances of G and AQ/G electrodes were investigated in 1 M KOH, the actual form of product in this study should be $HO_2^-$ ($pK_a(H_2O_2)$ = 11.75). The reactions were performed at each constant potential bias for 1 h, the FE values for $HO_2^-$ synthesis on AQ/G reached 90~95% over the tested potential range, while bare G exhibited FE values of 25~40%, which indicates the superior role of AQ in the 2-electron ORR process.

The EC activity of AQ in ORR process was further investigated using rotating ring-disk electrode (RRDE) experiments. RRDE technique is a well-established method to determine ORR activities, and it can estimate the electron transfer number (n) and $HO_2^-$ selectivity (%) based on RRDE current-potential curves and equations with ring and disk currents (*see* Fig. S3 for more details).[39,40] AQ/G samples exhibited n=2.0 and near 100% of $HO_2^-$ selectivity across a potential range, while bare G samples exhibited n~3.3 and ~40% of $HO_2^-$ selectivity (Fig. 1c and 1d). This clearly indicates that AQ anchored on the graphite rod plays a critical role for highly selective 2-electron ORR toward $HO_2^-$ synthesis, which is in good agreement with high FE of $HO_2^-$ synthesis on AQ/G electrode (Fig. 1b).

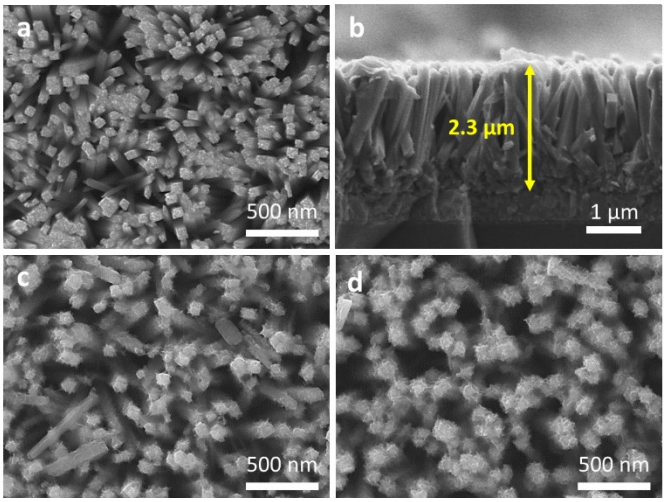


**Figure 2**. SEM images of bare TNR at (a) top view and (b) cross-sectional view, (c) fresh $RuO_x$-deposited TNR ($RuO_x$/TNR), and (d) used $RuO_x$/TNR over 100 h.

**Water photooxidation on $RuO_x$-deposited $TiO_2$ nanorod that provides electrons and protons**

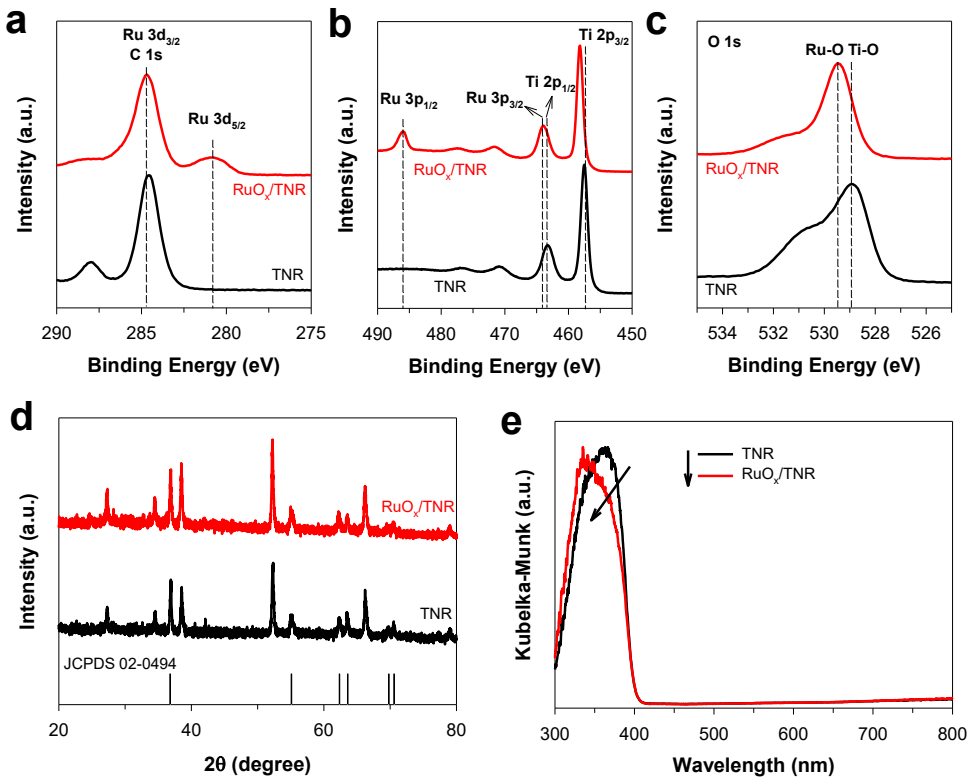


**Figure 3**. XPS spectra of (a) C 1s and Ru 3d, (b) Ti 2p and Ru 3p, and (c) O 1s for TNR and $RuO_x$/TNR. (d) XRD patterns of TNR and $RuO_x$/TNR. The reference peaks represent rutile $TiO_2$. (e) UV-vis diffusion reflectance absorption spectra of bare TNR and $RuO_x$/TNR. All spectra were expressed with Kubelka-Munk (K.M.) unit (K.M. = $(1-R^2)/2R$, where R represents the reflectance of the sample).

The $TiO_2$ nanorod (TNR) synthesized via hydrothermal method exhibited typical rectangular bunched morphology with ~50 nm width and ~2.3 μm length (Fig. 2a and 2b). The deposition of $RuO_x$ on TNR ($RuO_x$/TNR) induced a slight change in morphology, resulting in the deposition of needle-like structures on the nanorod arrays (Fig. 2c). The XPS spectra of Ru 3d and Ru 3p for $RuO_x$/TNR samples confirmed the presence of Ru element on TNR, while bare TNR exhibited no apparent peaks in the spectra (Fig. 3a and 3b). The XPS spectra of Ti 2p for $RuO_x$/TNR samples exhibited a slight shift to higher binding energy compared to that of bare TNR, indicating the interaction between $RuO_x$ and $TiO_2$ (Fig. 3b). The XPS O 1s bands for TNR and $RuO_x$/TNR also exhibited the similar binding energy shift between the two samples, showing 0.61 and 0.60 eV for Ti $2p_{1/2}$ and O 1s, respectively) (Fig. 3c). XRD patterns of TNR and $RuO_x$/TNR samples exhibited identical rutile $TiO_2$ peaks with predominant (101) plane at 36.8º (Fig. 3d), indicating that the formation of $RuO_x$ catalysts on TNT did not affect the crystalline phase. In addition, there were no additional peaks associated with the deposition of $RuO_x$ on TNR, which implies the amorphous nature of $RuO_x$ phase. The loading of $RuO_x$ talysts had a minimal effect on the optical properties of TNR (Fig. 3e).

The PEC performances of bare TNR and $RuO_x$/TNR samples were investigated using linear sweep voltammetry (LSVs) in 1 M

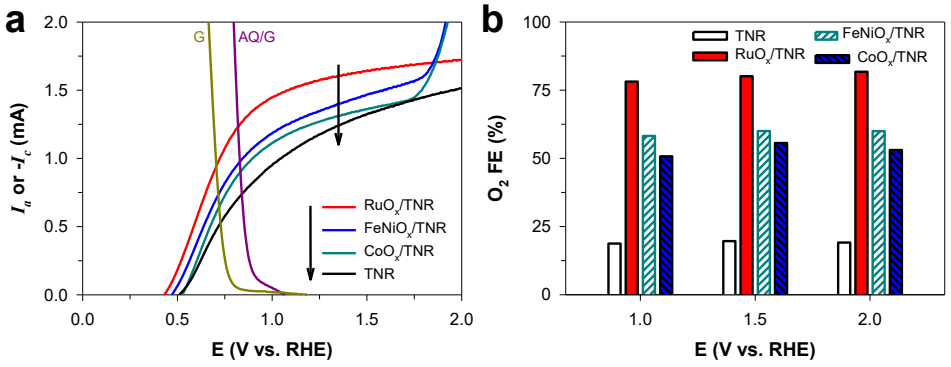


**Figure 4**. (a) Linear sweep voltammograms (LSVs) of bare TNR, $RuO_x$/TNR, $FeNiO_x$/TNR, and $CoO_x$/TNR in 1 M $H_2SO_4$. For comparison, cathodic currents of bare G and AQ/G under $O_2$ saturation (from Figure 1b) are also shown. (b) The Faradaic efficiencies (FEs) for $O_2$ evolution at various potential bias. The reaction was performed for 1 h. All experiments were performed under solar simulating condition (AM 1.5G, 100 $mWcm^{-2}$).

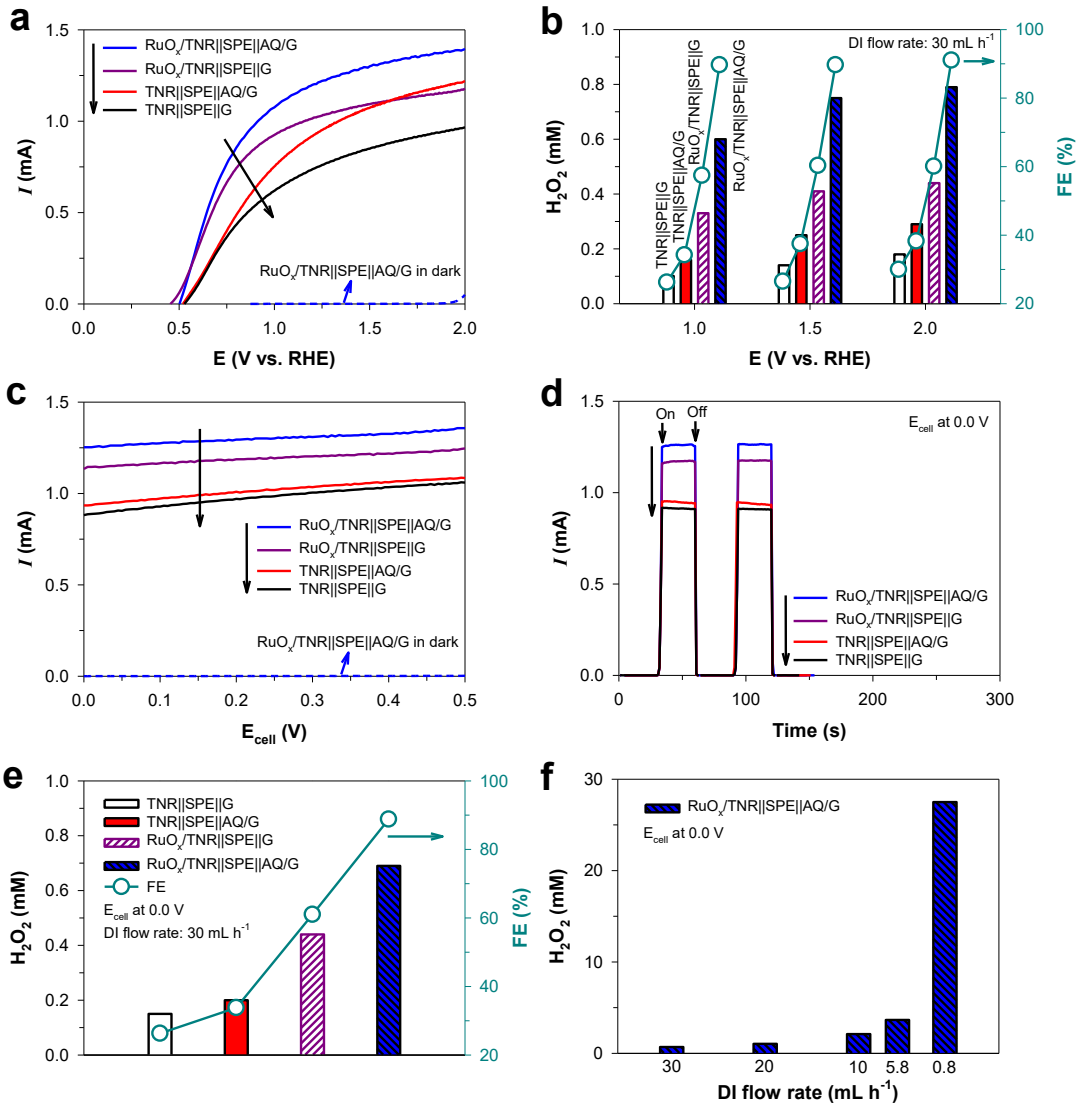


**Figure 5**. (a) Linear sweep voltammograms (LSVs) and (b) In-situ generated $H_2O_2$ concentration (mM) in the PEC cells with solid polymer electrolyte (SPE) in various electrode configurations (three-electrode system) at different potential bias. The reaction at each potential was performed for 1 h with DI water flow rate of 30 mL $h^{-1}$. (c) LSVs of the SPE-PEC cells in a two-electrode system. (d) Photocurrent-time profiles at $E_{cell}$ = 0.0 V. (e) $H_2O_2$ concentration (mM) generated with various electrode configurations at $E_{cell}$ = 0.0 V for 1 h. (f) $H_2O_2$ concentration (mM) obtained in the $RuO_x$/TNR||SPE||AQ/G cell (at $E_{cell}$ = 0.0 V for 1 h) under different DI water flow rates. All experiments were performed under solar simulating condition (AM 1.5G, 100 mW $cm^{-2}$). For comparison, the electrochemical activities of $RuO_x$/TNR||SPE||AQ/G configuration in three-electrode and two-electrode system are also shown in (a) and (c), respectively.

$H_2SO_4$ (pH ~0.15) solution purged with Ar under solar simulating condition (AM 1.5G, 100 mW $cm^{-2}$) (Fig. 4a). The LSVs of $RuO_x$/TNR exhibited superior performance for WOR to that of TNR. The deposition of $RuO_x$ on TNR induced both a negative shift (-0.1 $V_{RHE}$) in the onset potential and a higher photocurrent. The operation parameters under the bias-free condition can be predicted by comparing the LSVs of the photoanode and the cathode, which were obtained separately in the three-electrode system. The intersection point of LSV curves of the photoanode and the cathode indicates the ideal bias-free photocurrent when combining the two electrodes.[41,42] The photoanodic current of $RuO_x$/TNR and the cathodic current of AQ/G under $O_2$ saturation intersect at 1.23 mA and 0.81 V, indicating that this electrode configuration can operate without an external potential bias. The FEs for $O_2$ evolution via WOR were much higher for $RuO_x$/TNR than bare TNR (Fig. 4b). In addition, $CoO_x$ and $FeNiO_x$ were also prepared and tested as a co-catalyst on TNR, which are well-known water oxidation catalysts.[43-45] $CoO_x$/TNR and $FeNiO_x$/TNR exhibited higher photocurrent and higher FE ($O_2$) than bare TNR, but lower than $RuO_x$/TNR.

### PEC synthesis of pure $H_2O_2$ solution

To produce pure aqueous $H_2O_2$ solution that does not contain electrolytes, a PEC system that employed solid polymer electrolyte (SPE) was designed (Scheme 1). The PEC performances of various combined configurations using the photoanodes (TNR and $RuO_x$/TNR) and the cathode (G and AQ/G) were investigated using LSVs under solar simulating irradiation. The anode and cathode compartments contained 1

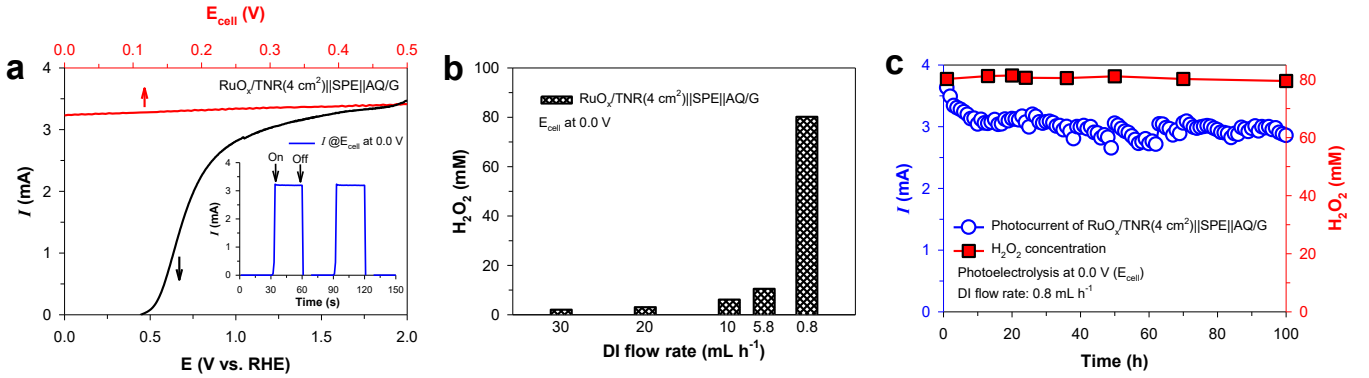


**Figure 6**. (a) Linear sweep voltammograms (LSVs) of the $RuO_x$/TNR||SPE||AQ/G configuration with a larger photoanode (4 $cm^2$ instead of 1 $cm^2$) in the three-electrode (black curve) and the two-electrode (red curve) system. The inset shows photocurrent generation in the two-electrode system at $E_{cell}$ = 0.0 V. (b) $H_2O_2$ concentration (mM) obtained in the $RuO_x$/TNR||SPE||AQ/G cell (at $E_{cell}$ = 0.0 V for 1 h) under different DI water flow rates. (c) Durability test for the continuous synthesis of $H_2O_2$ at $E_{cell}$ = 0.0 V over 100 h. All experiments were performed under solar simulating condition (AM 1.5G, 100 mW $cm^{-2}$).

M $H_2SO_4$ and 1 M KOH purged with $O_2$, respectively, with the SPE layer in a middle compartment through which DI water flowed. The electrode configuration using $RuO_x$/TNR and AQ/G exhibited the highest photocurrent generation (Fig. 5a), which is consistent with the enhanced (photo)electrochemical performances of $RuO_x$/TNR photoanode and AQ/G cathode. This enhanced PEC performance of $RuO_x$/TNR||SPE||AQ/G configuration should be attributed to the combined action of WOR and ORR on the photoanode and the cathode, which produces $H^+$ and $HO_2^-$ ions, respectively. These ions generated on the electrode surface transport into the middle compartment through the proton exchange membrane and the anion exchange membrane, respectively, and subsequently recombine to form $H_2O_2$. The resulting $H_2O_2$ is then dissolved into flowing DI water. The SPE layer can shuttle ions between the photoanode and the cathode in a solid phase instead of using liquid electrolyte. As SPE is the ion-conducting layer, its presence facilitates the ion transport and the recombination between $H^+$ and $HO_2^-$ ions in the middle compartment, which help maintain the neutral pH in the middle compartment. Without the SPE layer in the middle compartment, the PEC cell would suffer from high resistance between the photoanode and the cathode and slow ionic transportation. In addition, as SPE is insoluble to water and have porous structure, pure $H_2O_2$ can be formed and collected by water flow through SPE. The concentrations of pure aqueous $H_2O_2$ (electrolyte-free) collected in the PEC-SPE system were measured and compared among various electrode configurations (Fig. 5b). The $RuO_x$/TNR||SPE||AQ/G configuration yielded not only the highest concentration of $H_2O_2$ (~0.8 mM), but also the highest FE (~90%) in the tested potential range. These results clearly indicate that the enhanced performance of $RuO_x$/TNR for the production of $H^+$ by WOR and AQ/G for the production of $HO_2^-$ by ORR, leads to the high-yield synthesis of $H_2O_2$.

The PEC performances of the configuration using $RuO_x$/TNR and AQ/G electrodes were also investigated without the SPE layer in the middle compartment (Fig. S4). The configuration without SPE in the middle compartment, in which only DI water flows through middle compartment, exhibited unstable photocurrents. In addition, it was observed that electrolytes in the anode and cathode compartments leaked into the middle compartment without SPE through membranes, resulting in the pH change in the anode and cathode compartments. On the other hand, the neutral pH of the middle compartment solution could be maintained in the presence of SPE while it changed to alkaline pH without SPE. This clearly indicates that the presence of SPE layer could inhibit the transportation of undesired cation ($K^+$) and anion ($SO_4^{2-}$) into the middle compartment. Although $OH^-$ can transport through the anion exchange membrane along with $HO_2^-$, $OH^-$ ions immediately recombine with $H^+$ ions (to form $H_2O$) which transport into the SPE layer from the anode compartment (1 M $H_2SO_4$) through the proton exchange membrane. As a result, the middle compartment where pure $H_2O_2$ solution was generated maintained the neutral pH condition during the continuous PEC reaction and continuously generated a concentrated $H_2O_2$ solution during 100 h irradiation (*see* Figure 6c).

The PEC performances of the configurations were further investigated using LSVs under irradiation in a two-electrode system (Fig. 5c). The potential was directly applied between the photoanode and the cathode, which is indicated as the cell voltage ($E_{cell}$). The $RuO_x$/TNR||SPE||AQ/G configuration also exhibited the highest photocurrents and the photocurrents of 1.23 mA were generated for $RuO_x$/TNR||SPE||AQ/G configuration even under the bias-free condition (at $E_{cell}$ = 0.0 V) (Fig. 5d) as it is predicted in Fig. 4a as an operating point under the bias-free condition. On the other hand, there is a chemical bias (~0.8 V) developed between the photoanode and the cathode due to the pH difference (pH 0 *vs.* pH 14) of the electrolyte solutions even in the absence of the applied electrical bias, which could be a factor contributing to the high PEC efficiency under electrical bias-free condition. Synthesis of $H_2O_2$ could also be achieved under the bias-free condition, and the $RuO_x$/TNR||SPE||AQ/G configuration generated $H_2O_2$ concentration of ~0.7 mM with FE of ~90% (Fig. 5e). The concentration of in-situ generated $H_2O_2$ solution could be controlled by changing the DI water flow rate in the middle compartment (Fig. 5f). Using the optimized configuration (i.e., $RuO_x$/TNR||SPE||AQ/G), a maximal $H_2O_2$ concentration of ~30 mM was obtained at a DI flow rate of 0.8 mL $h^{-1}$.

A higher concentration level of $H_2O_2$ production could be achieved by using a larger photoanode ($RuO_x$/TNR with the surface area of 4 $cm^2$ instead of 1 $cm^2$) in the $RuO_x$/TNR||SPE||AQ/G configuration. LSVs of the larger photoanode show that higher photocurrents could be obtained in both three-electrode and two-electrode systems (Fig. 6a). Production of $H_2O_2$ under the bias-free condition could reach up to ~80 mM in 1 h irradiation by varying the DI water flow rate (Fig. 6b). The durability of the PEC cell was also investigated at the bias-free condition (Fig. 6c). A stable photocurrent of ~3 mA was maintained under a prolonged irradiation over 100 h while continuously producing ~80 mM level of $H_2O_2$ under the DI flow rate of 0.8 mL $h^{-1}$. This clearly demonstrates that production of pure $H_2O_2$ solution could successfully be obtained in an engineered PEC system using sunlight as a sole energy source and the scale-up of the photoanode should produce higher concentrations (beyond mM level) of $H_2O_2$ solution. The surface morphology of the photoanode after 100 h operation exhibited no sign of erosion (Fig. 2d).

## Conclusions

Previous studies of PEC systems for the synthesis of $H_2O_2$ have employed a batch cell where the in-situ produced $H_2O_2$ is present with undesired ions (*e.g.,* electrolytes), and further energy-intensive purification processes that may generate hazardous waste streams are needed to obtain high purity $H_2O_2$. Here we designed a new PEC system of a three-compartment cell which consists of a photoanode compartment, a cathode compartment, and an intervening SPE compartment. The three-compartment cell initiates water oxidation to produce $H^+$ in the photoanode ($RuO_x$/TNR) compartment and oxygen reduction to generate $HO_2^-$ in the cathode (AQ/G) compartment, and subsequently recombines $H^+$ and $HO_2^-$ to form pure (electrolyte-free) $H_2O_2$ in a SPE compartment with the continuous flow of DI water. $H^+$ and $HO_2^-$ ions are selective transported into the SPE compartment through PEM and AEM, respectively. The DI water flows through the middle SPE compartment and dissolves out as-formed $H_2O_2$ to obtain pure $H_2O_2$ solution.

The PEC synthesis of pure $H_2O_2$ solution could be successfully achieved under the external bias-free (0.0 V of cell voltage) condition using sunlight as a sole external energy source, while producing a continuous flow of ~80 mM $H_2O_2$ solution over 100 h with showing no sign of photocurrent decline. The performance of the present PEC system achieved a significantly higher $H_2O_2$ concentration than previous studies (Table 1). Note that all the previous studies produced $H_2O_2$ solutions mixed with electrolytes while this work generated pure $H_2O_2$ solution. However, the solar-to-$H_2O_2$ conversion efficiency of the three-compartment PEC cell was only ~0.42%, which is mainly ascribed to the low solar absorption capacity of TNR. With the employment of visible light-absorbing photoanodes, there should be more room for further improvements. More studies with the optimized (photo)electrodes combination are needed for better performance. In addition, although this system can produce pure $H_2O_2$ solution under a bias-free condition, the three-compartments PEC system also suffers from resistance from stacking for the high current collection, low ion conductivity of SPE, and instability of membranes for long-term operation. Further studies should attempt to overcome these drawbacks.

## Conflicts of interest

There are no conflicts to declare.

## Acknowledgements

This research was financially supported by the Leading Researcher Program (NRF-2020R1A3B2079953), which was funded by the Korea government (MSIT) through the National Research Foundation of Korea (NRF). The authors would like to thank Dr. Hyunwoong Park (Kyungpook National University) and Sunghun Kim for technical supports with photoelectrochemical cell and membranes.

## References

1 G. Strukul, *Catalytic oxidations with hydrogen peroxide as oxidant*, Springer Science & Business Media, 2013.
2 N. Agarwal, S. J. Freakley, R. U. McVicker, S. M. Althahban, N. Dimitratos, Q. He, D. J. Morgan, R. L. Jenkins, D. J. Willock and S. H. Taylor, *Science*, 2017, **358**, 223-227.
3 R. Hage and A. Lienke, *Angew. Chem. Int. Ed.*, 2006, **45**, 206-222.
4 A. D. Bokare and W. Choi, *J. hazard. Mater.*, 2014, **275**, 121-135.
5 H. Kim, J. Lim, S. Lee, H.-H. Kim, C. Lee, J. Lee and W. Choi, *Environ. Sci. Technol.*, 2019, **53**, 2918-2925.
6 J. M. Campos-Martin, G. Blanco-Brieva and J. L. Fierro, *Angew. Chem. Int. Ed.*, 2006, **45**, 6962-6984.
7 Q. Chen, *Chem. Eng. Process*, 2008, **47**, 787-792.
8 R. J. Lewis and G. J. Hutchings, *ChemCatChem*, 2019, **11**, 298-308.
9 S. J. Freakley, Q. He, J. H. Harrhy, L. Lu, D. A. Crole, D. J. Morgan, E. N. Ntainjua, J. K. Edwards, A. F. Carley and A. Y. Borisevich, *Science*, 2016, **351**, 965-968.
10 J. K. Edwards, E. Ntainjua N, A. F. Carley, A. A. Herzing, C. J. Kiely and G. J. Hutchings, *Angew. Chem. Int. Ed.*, 2009, **48**, 8512-8515.
11 S. Hu, *Sustainable Energy Fuels*, 2019, **3**, 101-114.
12 T. H. Jeon, H. Kim, H.-i. Kim and W. Choi, *Energy Environ. Sci.*, 2020, **13**, 1730-1742.
13 K. Fuku, Y. Miyase, Y. Miseki, T. Funaki, T. Gunji and K. Sayama, *Chem. Asian J.*, 2017, **12**, 1111-1119.
14 K. Zhang, J. Liu, L. Wang, B. Jin, X. Yang, S. Zhang and J. H. Park, *J. Am. Chem. Soc.*, 2020, **142**, 8641-8648.
15 D. S. Choi, H. Lee, F. Tieves, Y. W. Lee, E. J. Son, W. Zhang, B. Shin, F. Hollmann and C. B. Park, *ACS Catal.*, 2019, **9**, 10562-10566.
16 J. Liu, Y. Zou, B. Jin, K. Zhang and J. H. Park, *ACS Energy Lett.*, 2019, **4**, 3018-3027.
17 X. Shi, S. Siahrostami, G.-L. Li, Y. Zhang, P. Chakthranont, F. Studt, T. F. Jaramillo, X. Zheng and J. K. Nørskov, *Nat. Commun.*, 2017, **8**, 701.
18 P. Zhang, Y. W. Tong, Y. Liu, J. J. M. Vequizo, H. W. Sun, C. Yang, A. Yamakata, F. T. Fan, W. Lin, X. C. Wang and W. Choi, *Angew. Chem. Int. Ed.*, 2020, **59**, 16209-16217.

19 P. Zhang, D. Sun, A. Cho, S. Weon, S. Lee, J. Lee, J. W. Han, D.-P. Kim and W. Choi, *Nat. Commun.*, 2019, **10**, 940.
20 G.-h. Moon, M. Fujitsuka, S. Kim, T. Majima, X. Wang and W. Choi, *ACS Catal.*, 2017, **7**, 2886-2895.
21 G.-h. Moon, W. Kim, A. D. Bokare, N.-e. Sung and W. Choi, *Energy Environ. Sci.*, 2014, **7**, 4023-4028.
22 X. Shi, Y. Zhang, S. Siahrostami and X. Zheng, *Adv. Energy Mater.*, 2018, **8**, 1801158.
23 F. Ye, T. Wang, X. Quan, H. Yu and S. Chen, *Chem. Eng. J.*, 2020, **389**, 123427.
24 M. Ko, Y. J. Sa, J. Woo, T. V. T. Nguyen, J. H. Kim, D. Oh, P. Sharma, J. Ryu, T. J. Shin and S. H. Joo, *Nat. Commun.*, 2019, **10**, 5123.
25 W. Fan, B. Zhang, X. Wang, W. Ma, D. Li, Z. Wang, M. Dupuis, J. Shi, S. Liao and C. Li, *Energy Environ. Sci.*, 2020, **13**, 238-245.
26 K. Mase, M. Yoneda, Y. Yamada and S. Fukuzumi, *Nat. Commun.*, 2016, **7**, 11470.
27 I. Yamanaka, S. Tazawa, T. Murayama, T. Iwasaki and S. Takenaka, *ChemSusChem*, 2010, **3**, 59-62.
28 T. Murayama and I. Yamanaka, *J. Phys. Chem. C*, 2011, **115**, 5792-5799.
29 I. Yamanaka and T. Murayama, *Angew. Chem. Int. Ed.*, 2008, **120**, 1926-1928.
30 S. J. You, J. Y. Wang, N. Q. Ren, X. H. Wang and J. N. Zhang, *ChemSusChem*, 2010, **3**, 334-338.
31 J. Choi, S. H. Hwang, J. Jang and J. Yoon, *Electrochem. Commun.*, 2013, **30**, 95-98.
32 C. Xia, Y. Xia, P. Zhu, L. Fan and H. Wang, *Science*, 2019, **366**, 226-231.
33 B. Liu and E. S. Aydil, *J. Am. Chem. Soc.*, 2009, **131**, 3985-3990.
34 S. Kim, G. Piao, D. S. Han, H. K. Shon and H. Park, *Energy Environ. Sci.*, 2018, **11**, 344-353.
35 A. Sarapuu, K. Vaik, D. J. Schiffrin and K. Tammeveski, *J. Electroanal. Chem.*, 2003, **541**, 23-29.
36 G. Pognon, T. Brousse, L. Demarconnay and D. Bélanger, *J. Power Sources*, 2011, **196**, 4117-4122.
37 T. Yano, D. Tryk, K. Hashimoto and A. Fujishima, *J. Electrochem. Soc.*, 1998, **145**, 1870.
38 J. Zhang and L. Dai, *ACS Catal.*, 2015, **5**, 7244-7253.
39 R. Zhou, Y. Zheng, M. Jaroniec and S.-Z. Qiao, *ACS Catal.*, 2016, **6**, 4720-4728.
40 K. Jiang, S. Back, A. J. Akey, C. Xia, Y. Hu, W. Liang, D. Schaak, E. Stavitski, J. K. Nørskov and S. Siahrostami, *Nat. Commun.*, 2019, **10**, 3997.
41 Y. Surendranath, D. K. Bediako and D. G. Nocera, *PNAS*, 2012, **109**, 15617-15621.
42 J. H. Kim, D. Hansora, P. Sharma, J.-W. Jang and J. S. Lee, *Chem. Soc. Rev.*, 2019, **48**, 1908-1971.
43 X. Deng and H. Tüysüz, *ACS Catal.*, 2014, **4**, 3701-3714.
44 K. Fominykh, P. Chernev, I. Zaharieva, J. Sicklinger, G. Stefanic, M. Döblinger, A. Müller, A. Pokharel, S. Böcklein and C. Scheu, *ACS Nano*, 2015, **9**, 5180-5188.
45 R. D. Smith, M. S. Prévot, R. D. Fagan, Z. Zhang, P. A. Sedach, M. K. J. Siu, S. Trudel and C. P. Berlinguette, *Science*, 2013, **340**, 60-63.